ELSEVIER

Biophysical Chemistry 134 (2008) 101 – 109

Biophysical Chemistry

http://www.elsevier.com/locate/biophyschem

Self-assembly of electroactive layer-by-layer films of heme proteins with anionic surfactant dihexadecyl phosphate

Wenjing Shan, Hongyun Liu, Jiantao Shi, Lingzhu Yang, Naifei Hu *

Department of Chemistry, Beijing Normal University, Beijing 100875, China

Received 4 December 2007; received in revised form 28 January 2008; accepted 28 January 2008
Available online 6 February 2008

Abstract

Anionic surfactant dihexadecyl phosphate (DHP) with two hydrocarbon chains can be self-assembled into a double-layer structure with tail-to-tail configuration and negatively charged head groups toward outside in its aqueous dispersion. Due to this unique biomembrane-like structure, the "charge reversal" in DHP adsorption on solid surface was realized, and the DHP was successfully assembled with positively charged myoglobin (Mb) or hemoglobin (Hb) into $\{DHP/protein\}_n$ layer-by-layer films. Quartz crystal microbalance (QCM), UV–vis spectroscopy, and cyclic voltammetry (CV) were used to monitor or confirm the film assembly process. The $\{DHP/protein\}_n$ films grown on pyrolytic graphite (PG) electrodes showed a pair of well-defined and nearly reversible CV peaks at about −0.35 V vs SCE in pH 7.0 buffers, characteristic of the protein heme Fe(III)/Fe(II) redox couples. Based on the direct electrochemistry of heme proteins, the $\{DHP/protein\}_n$ films could also be used to electrochemically catalyze reduction of oxygen, hydrogen peroxide and nitrite with significant lowering of reduction overpotentials. Scanning electron microscopy (SEM), UV–vis spectroscopy, and reflectance absorption infrared (RAIR) spectroscopy were employed to characterize the $\{DHP/protein\}_n$ films, suggesting that the proteins in the films retain their near-native structure.

Keywords: Myoglobin; Hemoglobin; Dihexadecyl phosphate; Layer-by-layer assembly; Direct electrochemistry

1. Introduction

The study of direct electrochemistry of redox enzymes may provide a model or mimetic process for investigating the mechanism of electron transfer through redox chains of enzymes in biological systems, and establish a foundation for fabricating the new kind of biosensors or enzymatic bioreactors without using mediators [1,2]. However, it is usually difficult for redox proteins or enzymes in solution phase to transfer electrons directly with bare or naked solid electrodes. Various kinds of films modified on electrode surface may provide a favorable microenvironment for proteins, and the direct electrochemistry of some redox proteins in the film phase has been realized [3,4].

Among the different types of film-forming approaches, the layer-by-layer assembly technique has aroused increasing interests among researchers. Originally, the layer-by-layer assembly is based on alternate adsorption of oppositely charged polyelectrolytes on solid surface from their solutions [5,6]. For example, polycations can be adsorbed on the negatively charged surface by electrostatic interaction, and extra positive charges of the polycation layer will cause the surface charges to reverse from negative to positive. This "charge reversal" will make the subsequent adsorption of polyanions become possible. By repeating this cycle, the extension of sequential adsorption of polycation/polyanion bilayers on the solid surface will be realized, forming the layer-by-layer films. Over cast and dip-coating methods, the layer-by-layer assembly shows advantage in the precise control of film composition and thickness according to a predesigned architecture. Compared with other molecularly controlled methods such as self-assembly monolayers (SAMs) and Langmuir–Blodgett membrane, the layer-by-layer assembly is much simpler and more versatile, and suitable to a more variety of solid substrates with different shapes. Recently, this technique has been extended to fabricate protein multilayer films [6–8], and the direct electrochemistry

* Corresponding author. Tel.: +86 10 5880 5498; fax: +86 10 5880 2075.
E-mail address: hunaifei@bnu.edu.cn (N. Hu).

0301-4622/$ - see front matter © 2008 Elsevier B.V. All rights reserved.
doi:10.1016/j.bpc.2008.01.008

of some proteins in their layer-by-layer films with polyelectrolytes or nanoparticles have been successfully realized [3,9,10]. However, there seems seldom report on assembly of protein layer-by-layer films with small molecules or ions because the charge reversal in adsorption is usually difficult for the low molecular weight species [11].

Dihexadecyl phosphate (DHP) is a kind of anionic water-insoluble surfactants with a negatively charged phosphatic head group and two long hydrocarbon chains [12]. When it is dispersed in water with proper concentration, many DHP molecules can be self-assembled into double-layer structured vesicles [13,14]. After the vesicles are adsorbed or cast on solid surfaces, the ordered double-layer structured films are formed [14–16]. This unique structure is very similar to the structure of biological membranes, in which the constituent lipids are arranged in the tail-to-tail configuration with the hydrophilic head groups toward outside and proteins are adsorbed onto the surface of or imbedded into the layers [16–18]. Thus, the double-layer structure formed by DHP or other surfactants is called biomimetic membrane [15,19]. This kind of biomembrane-like films also provides a possibility to realize "charge reversal" in layer-by-layer assembly. That is, while a single ionic surfactant carries only one negative (or positive) charge, the double-layer structure formed by plenty of surfactant molecules as a whole carries many negative (or positive) charges on its both sides of surface and can act as a polyanion (or polycation) in the assembly. The layer-by-layer assembly with different surfactants based on formation of the double-layer structure has been reported [18,20–22]. For instance, Li and co-workers studied the multilayer assembly of dimyristoylphosphatidic acid (DMPA) lipid with human serum albumin (HSA) protein on particle surfaces [20]. However, to the best of our knowledge, no study on DHP layer-by-layer assembly has been reported up to now.

Due to the biomembrane-like structure formed by DHP, the cast DHP films demonstrate good biocompatibility and have been used to immobilize proteins. In particular, some redox proteins or enzymes incorporated in the DHP films cast on the electrode surface display good and nearly reversible electrochemical responses [23–25]. For example, in our precious work [26], direct electrochemistry of myoglobin (Mb) in DHP–PDDA composite films cast on electrodes was realized and used to electrochemically catalyze the reduction of various substrates, where PDDA was cationic poly(diallyldimethylammonium).

In the present work, positively charged Mb and hemoglobin (Hb) at pH 5.0 were selected as model proteins, and used to assemble layer-by-layer films with anionic surfactant DHP. The assembly process of $\{DHP/protein\}_n$ multilayer films were monitored and confirmed by quartz crystal microbalance (QCM), UV–vis spectroscopy, and cycle voltammetry (CV). The direct electrochemistry of the proteins in $\{DHP/protein\}_n$ films assembled on electrode surface was realized and the electrocatalytic properties of the protein films toward different substrates, such as oxygen, hydrogen peroxide, and nitrite, were studied. Scanning electron microscopy (SEM), UV–vis and IR spectroscopy were also used to characterize the films and investigate the possible conformation change of the proteins in the films. While the electrochemistry of Hb in its layer-by-layer films with cationic surfactant didodecyldimethylammonium (DDAB) was reported in our previous work [18], the assembly of multilayer films of electroactive heme proteins with anionic surfactant such as DHP has not been studied. This work provides a different type of example that the protein layer-by-layer films could be assembled with ionic small-molecular surfactants by the formation of double-layer structure of the surfactants, which considerably expands the materials or substances used in layer-by-layer assembly. The present work also indicates that the self-assembled surfactant layer may provide a unique biomembrane-like environment for biomolecules including heme proteins, which would be helpful to design the new type of electrochemical biosensors or bioreactors based on the direct electrochemistry of enzymes.

2. Experimental

2.1. Chemicals

Horse heart myoglobin (Mb, MW 17,800), bovine hemoglobin (Hb, MW 66,000), dihexadecyl phosphate (DHP, MW 546.86), poly(diallyldimethylammonium) (PDDA, 20%), and 3-mercapto-1-propanesulfonate (MPS) were all from Sigma-Aldrich and used as received. Clear aqueous dispersions of 0.5 mg mL^{-1} DHP were prepared by ultrasonication of DHP in water for several hours. Hydrogen peroxide (H_2O_2, 30%) and sodium nitrite were from Beijing Chemical Engineering Plant. H_2O_2 was freshly prepared before being used. Other chemicals were of reagent grade. Buffers were 0.05 M citric acid (pH 3.0), acetic acid (pH 5.0), potassium dihydrogen phosphate (pH 7.0), or boric acid (pH 9.0), all containing 0.1 M KCl. pH values were adjusted to the desired value with dilute HCl or KOH solution. Water used was twice distilled.

2.2. Preparation of $\{DHP/protein\}_n$ films

Prior to use, basal plane pyrolytic graphite (PG, Advanced Ceramics, geometric area 0.16 cm^2) disk electrodes were polished in metallographic sandpaper of 400 grit while flushing with water. The electrodes were then ultrasonicated in pure water for 30 s and dried in air. The PG electrodes were immersed in positively charged PDDA solutions (3 mg mL^{-1}, containing 0.5 M NaCl) for 20 min and then washed with water and dried in air, forming a PDDA precursor layer on the PG surface. The PG/PDDA electrodes were then immersed in an aqueous dispersion of DHP (0.5 mg mL^{-1}) for 20 min to adsorb DHP layer. After being washed with pure water and dried in air, the electrodes were then immersed in Mb or Hb solutions (1 mg mL^{-1}) at pH 5.0, where the proteins have net positive surface charges [27,28]. This cycle was repeated to obtain $\{DHP/protein\}_n$ layer-by-layer films on PG/PDDA surface with the desired number of bilayers (n).

Gold-coated resonator electrodes for QCM were covered by a drop of freshly prepared "piranha" solution (3:7 volume ratio of 30% H_2O_2 and 98% H_2SO_4. *Caution: piranha solution should be handled with extreme care, and only small volumes*

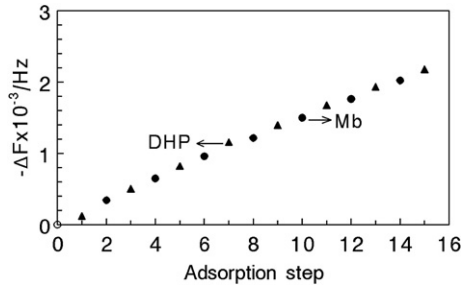

Fig. 1. Shift of QCM frequency with adsorption step of $\{DHP/Mb\}_n$ films on Au/MPS/PDDA surface: (○) PDDA adsorption step, (▲) DHP adsorption steps, and (●) Mb adsorption steps.

should be prepared at any time) on each side for 10 min at ca. 95 °C and then washed in pure ethanol and water successively. The cleaned gold electrodes were immersed in 4 mM MPS ethanol solutions for 24 h to form MPS monolayer on the gold surface and introduce negative charges on it. The following procedure to assemble the PDDA/$\{DHP/protein\}_n$ films on the Au/MPS surface was the same as on PG electrodes. After each adsorption step, the gold resonator electrodes were washed in water, dried in N_2 stream for 2 min to remove the adsorbed water, and then measured by QCM in air. Based on the Sauerbrey equation [29], $\Delta F = -2F_0^2 A^{-1}(\mu\rho_0)^{-1/2}\Delta m$, where F_0 is resonant frequency of the fundamental mode of the quartz crystal (8 MHz), μ is the shear modulus of quartz (2.947×10^{11} g cm^{-1} s^{-2}), ρ_0 is the density of the crystal (2.648 g cm^{-3}), and A is the geometric area of the QCM electrode (0.196 cm^2), the frequency shift, ΔF (Hz), would be proportional to the adsorbed mass, Δm (g). By taking into account the properties of quartz resonator used in this work, 1 Hz of frequency decrease corresponds to 1.35 ng of mass increase. If assuming that the layers were densely packed on the surface without any imperfection, the nominal thickness, d (cm), could be estimated by $d = -3.4\times10^{-9}\rho^{-1}\Delta F$, where ρ is the density of the adsorbed material (g cm^{-3}). For DHP, the density is around 1.2 ± 0.1 g cm^{-3} [30], while for the protein, the density is about 1.3 ± 0.1 g cm^{-3} [31].

The sample $\{DHP/protein\}_n$ films on QCM Au/MPS/PDDA electrodes were also used for SEM studies and reflectance absorption infrared (RAIR) spectroscopy. Quartz glass slides (1×4 cm, 1 mm thick) for UV–vis spectroscopy were washed in a washing solution (60% ethanol+39% water+1% KOH) for 30 min at 50 °C. After being rinsed with water and dried with N_2, PDDA/$\{DHP/protein\}_n$ films were then assembled on the quartz slides with the same way as on the PG electrodes.

2.3. Apparatus and procedures

A CHI 660B electrochemical workstation (CH Instruments) was used for CV and square wave voltammetry (SWV). The PG disk coated with films acted as the working electrode, a platinum flake as the counter, and a saturated calomel electrode (SCE) as the reference. The electrochemical measurements of the films were performed in buffers containing no protein. The buffers were purged with highly purified nitrogen for at least 15 min prior to a series of experiments. The nitrogen environment was then kept in the cell by continuously bubbling N_2 during the whole experiment. In aerobic experiments, measured volumes of air were injected into solutions in a sealed cell previously degassed with nitrogen.

A CHI 420 electrochemical analyzer (CH Instruments) was used for QCM. A Cintra 10e UV–visible spectrophotometer (GBC) was used for UV–vis absorption spectroscopy. SEM was performed with a JSM-6700F field emission scanning electron microscope (JEOL) at an acceleration voltage of 2 kV. About 10 nm of Au was coated onto the samples with an IB-3 ion coater (Eiko). RAIR spectra were obtained by using a Vatar 360 FT-IR (Nicolet) with a DTGS detector at 4 cm^{-1} resolution. All experiments were carried out at room temperature of 20 ± 2 °C.

3. Results and discussion

3.1. Assembly of $\{DHP/Mb\}_n$ films

The growth of $\{DHP/Mb\}_n$ layer-by-layer films was first monitored or confirmed by QCM (Fig. 1). A roughly linear decrease of frequency with adsorption step indicates that the adsorption amount of Mb and DHP in each bilayer is nearly the same, respectively, and the building-up of $\{DHP/Mb\}_n$ films is in a regular and reproducible manner. If assuming the layer was arranged compactly, the nominal thickness of Mb layer was about 3.2 nm, close to the molecular dimension of Mb ($2.5\times3.5\times4.5$ nm^3 [28]). This suggests that the adsorption of Mb is roughly monomolecular in each assembly cycle. The nominal thickness of DHP layer estimated by QCM was about 4.9 nm, which was around two times larger than the length of DHP molecule (2.3 nm [32]). This implies that the DHP molecules are most probably self-assembled into a tail-to-tail double-layer structure with the negatively charged head groups toward outside. This kind of biomembrane-like structure was also observed in other types of DHP films [13,14]. It is the adsorption of DHP double-layer structure as a whole in the assembly that causes the surface charge of the electrode to be reversed from positive to negative, making the following adsorption of positively charged Mb at pH 5.0 become possible. Thus, the electrostatic interaction between oppositely charged

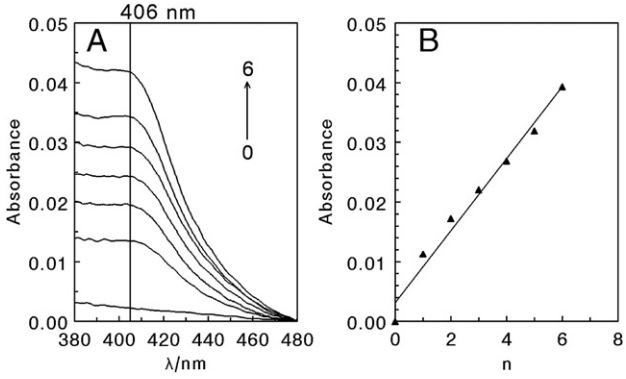

Fig. 2. (A) UV–vis spectra on quartz slides for dry PDDA/$\{DHP/Mb\}_n$ films with different number of adsorption cycles (n). (B) The dependence of the absorbance at 406 nm with n for $\{DHP/Mb\}_n$ films.

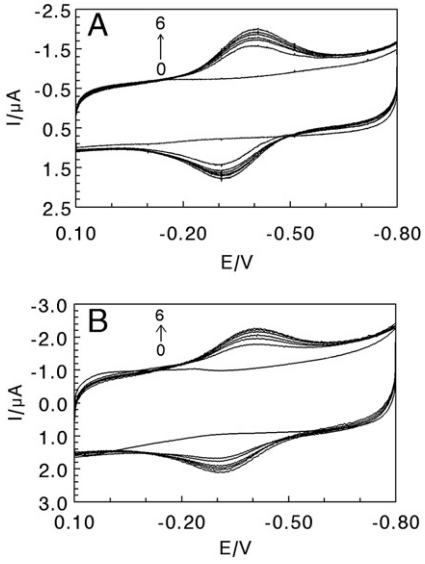

Fig. 3. CVs of (A) $\{DHP/Mb\}_n$ films and (B) $\{DHP/Hb\}_n$ films at 0.2 V s^{-1} in pH 7.0 buffers with different number of adsorption cycles (n).

Mb and DHP double-layer structure would be the main driving force for the assembly of $\{DHP/Mb\}_n$ films.

The growth of $\{DHP/Mb\}_n$ multilayer films was also confirmed by UV–vis spectroscopy (Fig. 2). After each adsorption cycle for DHP/Mb bilayer, the films fabricated on quartz slides were washed with water and dried in air, followed by UV–vis measurement. The Soret absorption band of Mb at 406 nm increased linearly with the number of bilayers (n), indicating that almost the same amount of Mb is adsorbed in each adsorption cycle. This result is consistent with that of QCM.

The $\{DHP/Mb\}_n$ films assembled on PG electrode surface were also tested by CV (Fig. 3A). After being abraded, the surface of basal plane PG became rough and the "edge" surface of PG was uncovered, which was negatively charged by virtue of the surface oxygen functionalities and had a partly hydrophobic character [33]. Thus, positively charged PDDA was directly adsorbed on the PG surface by both electrostatic and hydrophobic interactions. The PDDA precursor layer provided a relatively smooth surface for the adsorption of anionic DHP, and the formed negatively charged DHP double-layer structure on the surface would successively adsorb positively charged Mb at pH 5.0 through electrostatic attraction, forming the DHP/Mb bilayer. The cycle was repeated to assemble $\{DHP/Mb\}_n$ films on the electrodes. After each adsorption cycle, the $\{DHP/Mb\}_n$ film electrodes were placed in a pH 7.0 buffer containing no Mb, followed by CV scans. A pair of well-defined, quite reversible CV peaks was observed at about −0.35 V vs SCE. This peak pair should be attributed to the Fe(III)/Fe(II) redox couple for Mb prosthetic heme group according to the literature [3,4,9,10,16,17,23], in which the reversible CV redox peak pair of Mb in different kinds of films modified on electrodes at the similar position were also observed under the similar conditions. Both reduction and oxidation peaks of $\{DHP/Mb\}_n$ films grew with n at $n<6$, and then reached the steady state, indicating the successful assembly of the films at least when n is less than 6. In contrast, PG/PDDA/DHP film electrodes with no Mb adsorbed showed no CV response at all in the same potential window.

The $\{DHP/Hb\}_n$ films assembled layer-by-layer by Hb and DHP were also confirmed by CV (Fig. 3B), and showed very similar characters to the $\{DHP/Mb\}_n$ films.

3.2. Electrochemical properties of $\{DHP/protein\}_n$ films

For a specific $\{DHP/protein\}_n$ film with a certain n value, the CV in pH 7.0 buffers showed quite symmetric peak shapes and nearly equal reduction and oxidation peak heights (Fig. 3). The CV peak currents increased linearly with scan rate from 0.05 to 2.0 V s^{-1}, and the integration of reduction peaks at different scan rates in this range gave nearly constant charge values. All these are characteristic of diffusionless, surface-confined voltammetric behavior [34]. Thus, the integration of the CV reduction peak would give the amount of charge (Q) passing through the electrode for full reduction of the proteins in the films, and the Q value could be further converted to the surface concentration of electroactive protein (Γ^*, mol cm^{-2}) in the films according to the equation of $Q=NAF\Gamma^*$ based on the Faraday's law [34], where A is the geometric area of PG electrode, N is the number of electrons transferred, and F is the Faraday's constant. For both $\{DHP/Mb\}_n$ and $\{DHP/Hb\}_n$ films, the Γ^* value increased non-linearly with n up to 6, and tended to level off afterwards (Fig. 4a and b). From the QCM results, the average adsorption amount of Mb in each bilayer was about 2.4×10^{-11} mol cm^{-2}, while the surface concentration of electroactive Mb in the first DHP/Mb bilayer estimated by CV was about 2.5×10^{-11} mol cm^{-2}. Considering the experimental error and the difference in surface roughness between PG and QCM Au electrodes, these two values are reasonably close to each other, suggesting that almost all the Mb molecules in the first adsorption bilayer is electroactive. Taking this assumption, the fraction of electroactive Mb in the following bilayers could be estimated. While the adsorption amount of Mb in each adsorption cycle was almost the same according to the QCM and UV–vis spectroscopic results (Figs.

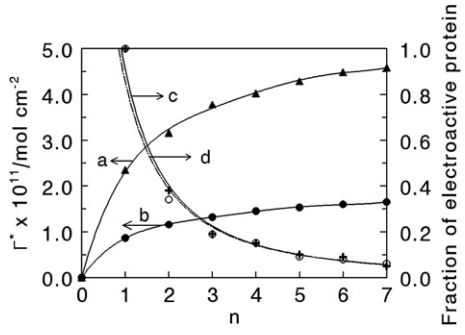

Fig. 4. Influence of the number of bilayers (n) on the surface concentration of electroactive proteins (Γ^*) (a and b) and the fraction of electroactive proteins (c (+) and d (○)) for $\{DHP/Mb\}_n$ (a and c) and $\{DHP/Hb\}_n$ (b and d) films. Γ^* was estimated by integration of CV reduction peak at 0.2 V s^{-1} in pH 7.0 buffers.

1 and 2), the fraction of electroactive Mb in each bilayer decreased dramatically with n (Fig. 4c). When the number of bilayers became larger than 6, the Mb molecules in the outer bilayers at $n>6$ were no longer electrochemically accessible. The $\{DHP/Hb\}_n$ films showed the similar behavior (Fig. 4d). These results indicate that the distance between the proteins and the electrode surface is crucial for the efficient electron exchange. The greater the distance, the less the percentage of the electroactive proteins would be.

This distance-dependent character of $\{DHP/protein\}_n$ films may be further rationalized in terms of the unique mechanism of electron transfer for redox proteins in film phase. Taking $\{DHP/Mb\}_n$ films as an example, the electroactive Mb can extend to about 6 bilayers, which approximately corresponds to the thickness of about 50 nm according to the QCM results. It is almost impossible for the macromolecular Mb to physically diffuse through such a long distance in the film phase, reach the electrode surface, and then exchange electron with underlying electrodes in the time scale of CV scan. Therefore, it is more reasonable for Mb in the films to take electron-hopping or electron self-exchange mechanism to exchange electron with underlying electrodes [35]. In electron-hopping, two neighboring Mb molecules inside the films exchange electron with each other, and the electron transfer of Mb can be extended sequentially from the electrode surface to the Mb molecules far away from the surface by successive electron hoping among the neighboring Mb molecules in the films. However, the electron transfer of Mb in the films has to be accompanied by transportation of electrochemically inert counterions from external solution into the films and/or from the films back to the solution in order to compensate the charge alteration caused by the electron transfer and maintain the electroneutralisation of the whole films. The efficiency of counterion transportation within film phase may thus become a controlling factor in overall charge transport in electroactive films [35]. When the $\{DHP/Mb\}_n$ films become thicker with a larger n value, the resistance of the films toward the diffusion of counterions would become higher, thus decreasing the efficiency of counterion transportation in the films and then limiting the corresponding electron transfer of Mb. This is most probably the reason why the electroactive heme proteins in $\{DHP/protein\}_n$ layer-by-layer films can only extend to about 6 bilayers.

Since both $\{DHP/Mb\}_n$ and $\{DHP/Hb\}_n$ films demonstrated the maximum CV responses and Γ^* value at $n=6$, in the following voltammetric experiments, the $\{DHP/protein\}_6$ films with $n=6$ were usually used to study the electrochemical properties of the films.

The $\{DHP/protein\}_6$ films showed good stability in blank buffers. Taking $\{DHP/Hb\}_6$ films as an example, after two weeks of storage in pH 7.0 buffers, the CV redox peak potentials of the $\{DHP/Hb\}_6$ films remained in the same positions, and the peak heights decreased about 15% compared with their initial values. Considering that the DHP is a small molecule, the stability of the films is very impressive. The good stability of the films also suggests that while the primary driving force of the film assembly is the electrostatic interaction between oppositely charged proteins and DHP double-layers, some non-electrostatic interactions such as hydrophobic interaction and hydrogen bonding may play an important role in stabilizing the films in the blank buffers.

SWV combined with non-linear regression analysis was used to estimate the apparent heterogeneous electron transfer rate constant (k_s) and formal potential ($E^{\circ\prime}$) for $\{DHP/protein\}_6$ films. The model used here was based on the Butler–Volmer equations [36] for diffusionless and thin-layer controlled system with the combination of the single-species surface-confined SWV model [37] and the formal potential dispersion model [23,38], which was described in detail previously [23,38]. The analysis of SWV data for $\{DHP/protein\}_6$ films demonstrated goodness of fit onto the model over a range of amplitudes and frequencies. The average k_s and $E^{\circ\prime}$ values obtained from fitting SWV data are listed in Table 1. Other electrochemical parameters of the films estimated by CV are also listed for comparison. The k_s values of $\{DHP/Mb\}_6$ and $\{DHP/Hb\}_6$ films were similar and in the same order as that of other Mb or Hb films [18,25,26]. These relatively large k_s values are qualitatively in agreement with the quasi-reversible CV behavior of the films. The $E^{\circ\prime}$ values obtained by SWV for $\{DHP/protein\}_n$ films were close to those estimated by CV, but might be different from those for the proteins in other types of films. This confirms that the film microenvironment and film components may influence the $E^{\circ\prime}$ values as reported previously [38].

CVs of $\{DHP/protein\}_6$ films showed great dependence on pH of external buffers. An increase of pH in solution led to a negative shift in potential of both reduction and oxidation peaks, while the surface concentration of electroactive proteins (Γ^*) maintained nearly constant. The formal potential ($E^{\circ\prime}$), estimated as the midpoint of reduction and oxidation peak potentials of the heme protein Fe(III)/Fe(II) redox couple, had a linear relationship with pH from pH 6.0 to 10.0 with a slope of -41.0 mV pH^{-1} for $\{DHP/Mb\}_6$ films, and -40.3 mV pH^{-1} for $\{DHP/Hb\}_6$ films. These slope values were smaller than the theoretical value of -58.1 mV pH^{-1} at 20 °C for a reversible proton-coupled single-electron transfer process [39]. The reason for this is not clear yet. But one thing for sure is that the electron transfer between heme proteins in $\{DHP/protein\}_6$ films and PG electrodes is accompanied by proton transportation. The $E^{\circ\prime}$ vs pH curve for both films showed an inflection point at pH 6.0. At pH lower than 6.0, $E^{\circ\prime}$ changed more slowly with pH with the slope of -30 mV pH^{-1} for both films. The linear dependence of $E^{\circ\prime}$ on pH of external solution was also observed for other heme protein films including cast protein–surfactant films [17], protein–surfactant–polyion composite films [25], and $\{protein/polyion\}_n$ layer-by-layer films [40]. However, the position of inflection point varied from films to films [17,25]. Some

Table 1
Electrochemical parameters of $\{DHP/protein\}_n$ films in pH 7.0 buffers

Films	Γ^*/(mol cm^{-2}) [a]	$E^{\circ\prime}$/V [a]	ΔE_p/V [a]	$E^{\circ\prime}$/V [b]	k_s/s^{-1} [b]
$\{DHP/Mb\}_6$	4.5×10^{-11}	−0.35	0.10	−0.37	43
$\{DHP/Hb\}_6$	1.7×10^{-11}	−0.36	0.11	−0.42	32

[a] Estimated by CVs at 0.2 V s^{-1}.
[b] Average values for analysis of SWV data obtained at frequencies of 100–200 Hz, amplitudes of 60 and 75 mV, and a step height of 4 mV.

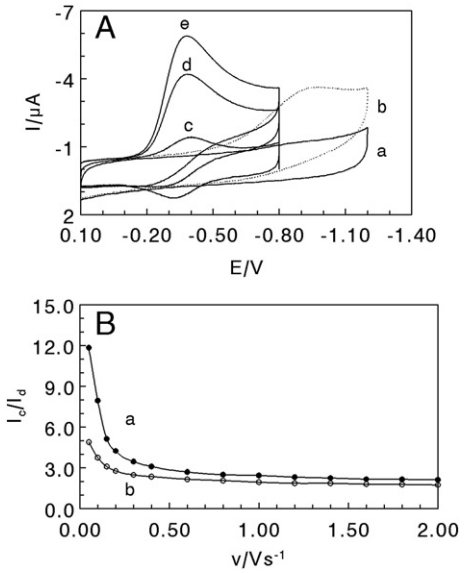

Fig. 5. (A) CVs at 0.1 V s^{-1} in 10 mL of pH 7.0 buffers for (a) PDDA/DHP films in the absence of O_2, (b) PDDA/DHP films after 3 mL of air was injected, (c) $\{DHP/Mb\}_6$ films in the absence of O_2, and $\{DHP/Mb\}_6$ films after (d) 3 mL and (e) 5 mL of air were injected. (B) Influence of scan rate on catalytic efficiency, I_c/I_d, for (a) $\{DHP/Mb\}_6$ and (b) $\{DHP/Hb\}_6$ films, where I_d was the CV reduction peak current in pH 7.0 buffers without oxygen and I_c was the CV reduction peak current after 10 mL of air was injected in 10 mL of pH 7.0 buffers.

system such as $\{Mb/PSS\}_n$ films even showed no inflection point at all over the entire pH range from 2.5 to 12.0 [40], where PSS was poly(styrene sulfonate). The exact reason for this is not known yet, but it must be related to the different microenvironment for the proteins provided by different films. The inflection point may reflect the apparent pK_a value of the protonatable sites of proteins associated with the electrode reaction [38,41], and the pK_a may be influenced by the different film environment. In addition, the proteins in films may be partially denatured in relatively acidic environment, which may also be one of the reasons why the inflection point appears in the $E^{\circ\prime}$ vs pH curve. Different types of films may stabilize the proteins to a different extent, resulting in the different position of the inflection point.

3.3. Electrocatalytic reactivity of $\{DHP/protein\}_6$ films

The electrocatalytic reactivity of $\{DHP/protein\}_6$ films toward oxygen, hydrogen peroxide and nitrite was investigated by CV. For instance, Mb in $\{DHP/Mb\}_6$ films showed good catalytic activity toward oxygen. When a volume of air was passed through a pH 7.0 oxygen-free buffer in a sealed cell by a syringe, a significant increase in the reduction peak at about −0.4 V was observed (Fig. 5A), accompanied by the disappearance of the oxidation peak of MbFe(II), suggesting that MbFe(II) had reacted with oxygen. An increase in the amount of oxygen in solution increased the reduction peak current. For the DHP film adsorbed on PG/PDDA, the peak for direct reduction of oxygen was observed at about −0.90 V. Thus, the $\{DHP/Mb\}_6$ films decreased the reduction overpotential of oxygen by 0.5 V. The catalytic efficiency expressed as the ratio of reduction peak current in the presence of oxygen (I_c) over that in the absence of oxygen (I_d), I_c/I_d, decreased with increase of scan rate (Fig. 5B), also characteristic of electrochemical catalysis of oxygen by $\{DHP/Mb\}_6$ films [42,43]. $\{DHP/Hb\}_6$ film electrodes showed similar catalytic property toward oxygen. With the same scan rate and the same volume of air injected, $\{DHP/Mb\}_6$ films demonstrated larger catalytic efficiency than the $\{DHP/Hb\}_6$ films (Fig. 5B).

Electrochemical catalysis of hydrogen peroxide was also observed at $\{DHP/protein\}_6$ film electrodes. For example, when H_2O_2 was added to a pH 7.0 buffer, an increase in the reduction peak at about −0.4 V for $\{DHP/Mb\}_6$ films was observed with the decrease of the oxidation peak as compared with the films with no H_2O_2 present (Fig. 6A). The reduction peak current increased with the concentration of H_2O_2 in solution, accompanied by the further decrease or even disappearance of the oxidation peak. In the meantime, no direct reduction peak was observed at PDDA/DHP film electrodes in the presence of H_2O_2. The CV reduction peak had a linear relationship with H_2O_2 concentration in the range of 2–65 μM, while at higher H_2O_2 concentration, the CV response did not increase anymore. The catalytic behavior of H_2O_2 at $\{DHP/Mb\}_6$ film electrodes was very similar to that of oxygen (Figs. 5A and 6A), implying the similarity of reaction mechanism between the two systems. This was also observed for other heme protein films, and the mechanism was discussed in detail in the previous publications [44,45].

Electrocatalytic reduction of NO_2^- was also studied by CV on $\{DHP/protein\}_6$ films. Taking $\{DHP/Hb\}_6$ films as an example. When NO_2^- was added into pH 5.0 buffers, a new reduction peak was observed at about −0.8 V (Fig. 6B). The reduction peak

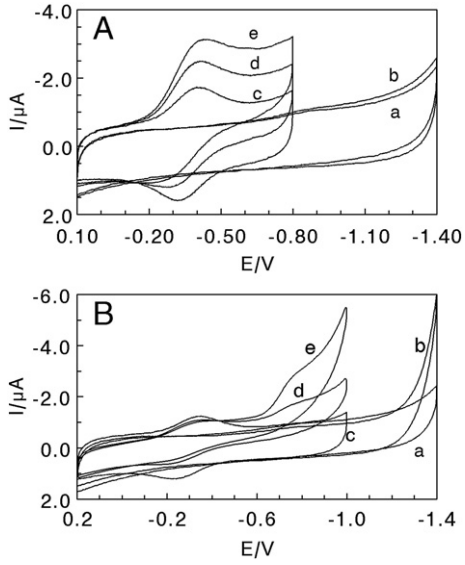

Fig. 6. (A) CVs at 0.2 V s^{-1} in pH 7.0 buffers for (a) PDDA/DHP films in buffers containing no H_2O_2, (b) PDDA/DHP films in buffers containing 10 μM H_2O_2, (c) $\{DHP/Mb\}_6$ films in buffers containing no H_2O_2, and $\{DHP/Mb\}_6$ films in buffers containing (d) 10 μM and (e) 20 μM H_2O_2. (B) CVs at 0.2 V s^{-1} in pH 5.0 buffers for (a) PDDA/DHP films in buffers containing no NO_2^-, (b) PDDA/DHP films in buffers containing 1.2 mM NO_2^-, (c) $\{DHP/Hb\}_6$ films in buffers containing no NO_2^-, and $\{DHP/Hb\}_6$ films in buffers containing (d) 1.2 mM and (e) 2.4 mM NO_2^-.

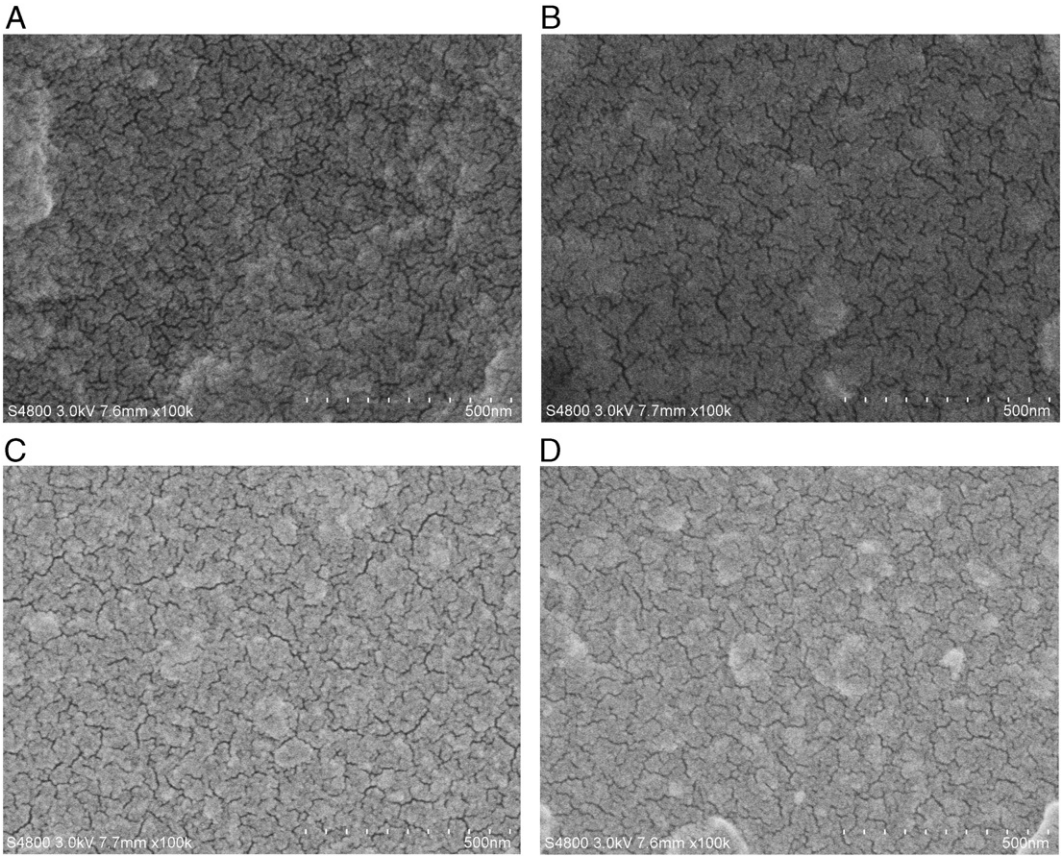

Fig. 7. SEM top views of (A) $\{DHP/Mb\}_9$, (B) $\{DHP/Hb\}_9$, (C) $\{DHP/Mb\}_9$/DHP, and (D) $\{DHP/Hb\}_9$/DHP films assembled on Au/MPS/PDDA surface.

current increased with the concentration of NO_2^- in solution. Direct reduction of NO_2^- on PDDA/DHP films was observed at the potential more negative than −1.2 V. Thus, $\{DHP/Hb\}_6$ films decreased reduction overpotential of NO_2^- by at least 0.4 V.

3.4. Structure feature of the films

The surface morphology of $\{DHP/protein\}_9$ films was characterized by SEM (Fig. 7). For both $\{DHP/Mb\}_9$ and $\{DHP/Hb\}_9$ films, a non-uniform surface with some aggregation or "particles" on it was observed. While there was no substantial difference between Mb and Hb films in the top-view SEM, the $\{DHP/Mb\}_9$ films seemed rougher than the $\{DHP/Hb\}_9$ films. The surface topography of $\{DHP/protein\}_9$/DHP films with DHP as the outermost layer (Fig. 7C and D) was compared with that of the films with the corresponding protein as the outermost layer (Fig. 7A and B). While the former seemed smoother than the latter, the two types of films showed no essential difference in morphology. This suggests that at least partial interlayer mixing or penetrating may happen between the DHP and protein adsorption layers in the assembly. For biomembrane-like films, protein molecules were not only adsorbed on the film surface but also imbedded in the bilayer structure [16,17], which may also take place in the $\{DHP/protein\}_n$ film system.

The shape and position of Soret absorption band of the heme prosthetic group in heme proteins may provide the information of protein conformation [46,47]. UV–vis spectroscopy was thus performed to study the possible denaturation of proteins in $\{DHP/protein\}_n$ films assembled on quartz slides. For example, dry $\{DHP/Hb\}_6$ films showed the Soret band at 411 nm, very close to that of dry Hb films alone [25] (Fig. 8A), indicating that the microenvironment that the films provide has no substantial influence on the conformation of incorporated Hb. When the $\{DHP/Hb\}_6$ films were placed into buffer solutions at pH 5.0, 7.0 and 9.0, respectively, the Soret band position remained at 411 nm and the peak kept the well-defined shape, suggesting

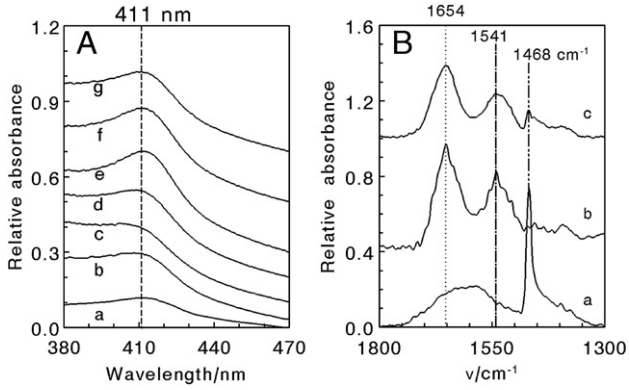

Fig. 8. (A) UV–vis absorption spectra of (a) dry PDDA/$\{DHP/Hb\}_6$ films on quartz slides and PDDA/$\{DHP/Hb\}_6$ films in different pH buffers: (b) pH 11.0, (c) pH 4.0, (d) pH 10.0, (e) pH 5.0, (f) pH 9.0, and (g) pH 7.0. (B) RAIR spectra of (a) cast DHP films, (b) cast Hb films, and (c) $\{DHP/Hb\}_9$ films assembled on Au/MPS/PDDA surface.

that Hb in the films essentially retains its near-native structure in the medium pH range. When pH of the buffer was changed toward a more acidic or basic direction, the Soret band showed a blue-shift with broadening of peak shape. At pH 4.0, for example, the Soret band shifted to 400 nm, and the distorted peak was even hardly observed (Fig. 8A, curve c). This suggests that at the relatively extreme pH, Hb in the films may be denatured to a great extent. The same results were also observed for the $\{DHP/Mb\}_6$ films.

RAIR spectroscopy was also used to detect conformational change of proteins in $\{DHP/protein\}_n$ films. Fig. 8B shows the typical RAIR spectra of pure DHP and Hb films cast on Al substrates and $\{DHP/Hb\}_9$ films assembled on Au/MPS/PDDA surface. Pure Hb films showed IR amide I band at 1653 cm^{-1} which was caused by C=O stretching vibration, and amide II band at 1541 cm^{-1} which was attributed to the combination of N–H in-plane bending and C–N stretching vibration [48,49]. The pure DHP films showed a sharp peak at 1468 cm^{-1}. All these three peaks were observed for the $\{DHP/Hb\}_9$ films, confirming that the DHP and Hb are successfully assembled into the layer-by-layer films. The positions of amides I and II bands for the $\{DHP/Hb\}_9$ films at 1654 and 1541 cm^{-1} were very close to those for pure Hb films, respectively, implying that the major portion of Hb essentially retains its native structure in the $\{DHP/Hb\}_9$ films.

4. Conclusions

Anionic small-molecular surfactant DHP can form layer-by-layer films with positively charged Mb or Hb at pH 5.0 mainly because the formation and adsorption of DHP double-layer structure make the surface charge of solid surface become reversed from positive to negative. This work provides a new example of assembly of $\{surfactant/protein\}_n$ layer-by-layer films, which may greatly expand the materials or substances used in the assembly of enzyme multilayers. The biomembrane-like DHP films provide a biocompatible microenvironment for the proteins, and the proteins in the $\{DHP/protein\}_n$ films demonstrate good and direct electrochemistry. Based on this, the protein films can be used to electrochemically catalyze the reduction of various substrates of biological or environmental significance, suggesting that the films have a promising potential in fabricating mediator-free biosensors or bioreactors.

Acknowledgement

The financial support from the National Natural Science Foundation of China (NSFC 20475008 and 20775009) and the Research Fund for the Doctoral Program of Higher Education of China (Project for Junior Faculty Members, 20070027021) is acknowledged.

References

[1] M.F. Chaplin, in: M.F. Chaplin, C. Bucke (Eds.), Enzyme Technology, Cambridge University Press, Cambridge, UK, 1990, pp. 1–40.
[2] F.A. Armstrong, H.A.O. Hill, N.J. Walton, Direct electrochemistry of redox proteins, Acc. Chem. Res. 21 (1998) 407–413.
[3] J.F. Rusling, Z. Zhang, in: R.W. Nalwa (Ed.), Handbook of Surfaces and Interfaces of Materials, vol. 5, Academic Press, New York, 2001, pp. 33–71.
[4] N. Hu, Direct electrochemistry of redox proteins or enzymes at various film electrodes and their possible applications in monitoring some pollutants, Pure Appl. Chem. 73 (2001) 1979–1991.
[5] G. Decher, Fuzzy nanoassemblies: toward layered polymeric multicomposites, Science 277 (1997) 1232–1237.
[6] Y. Lvov, in: R.W. Nalwa (Ed.), Handbook of Surfaces and Interfaces of Materials, vol. 3, Academic Press, San Diego, CA, 2001, pp. 170–189.
[7] Y. Lvov, in: Y. Lvov, H. Möhwald (Eds.), Protein Architecture: Interfacing Molecular Assemblies and Immobilization Biotechnology, Dekker, New York, 2000, pp. 125–166.
[8] Y. Lvov, F. Caruso, Biocolloids with ordered urease multilayer shells as enzymatic reactors, Anal. Chem. 73 (2001) 4212–4217.
[9] Y. Lvov, Z. Lu, J.B. Schenkman, X. Zu, J.F. Rusling, Direct electrochemistry of myoglobin and cytochrome P450cam in alternate layer-by-layer films with DNA and other polyions, J. Am. Chem. Soc. 120 (1998) 4073–4080.
[10] J.F. Rusling, in: Y. Lvov, H. Möhwald (Eds.), Protein Architecture: Interfacing Molecular Assemblies and Immobilization Biotechnology, Dekker, New York, 2000, pp. 337–354.
[11] L. Yang, H. Liu, N. Hu, Assembly of electroactive layer-by-layer films of myoglobin and small-molecular phytic acid, Electrochem. Commun. (2007) 1057–1061.
[12] S. Lukac, Surface potential at surfactant and phospholipid vesicles as determined by amphiphilic pH indicators, J. Phys. Chem. 87 (1983) 5045–5050.
[13] J.E. Melanson, N.E. Baryla, C.A. Lucy, Double-chained surfactants for semipermanent wall coatings in capillary electrophoresis, Anal. Chem. 72 (2000) 4110–4114.
[14] T.F. Svitova, Y.P. Smirnova, S.A. Pisarev, N.A. Berezina, Self-assembly in double-tailed surfactants in dilute aqueous solutions, Colloids Surf., A 98 (1995) 107–115.
[15] A. Kotyk, K. Janacek, J. Koryta, Biophysical Chemistry of Membrane Function, Wiley, Chichester, UK, 1988.
[16] J.F. Rusling, Enzyme bioelectrochemistry in cast biomembrane like films, Acc. Chem. Res. 31 (1998) 363–369.
[17] J.F. Rusling, A.-E.F. Nassar, Enhanced electron transfer for myoglobin in surfactant films on electrodes, J. Am. Chem. Soc. 115 (1993) 11891–11897.
[18] Y. Hu, H. Sun, N. Hu, Assembly of layer-by-layer films of electroactive hemoglobin and surfactant didodecyldimethylammonium bromide, J. Colloid Interface Sci. 314 (2007) 131–140.
[19] G. Cevc, D. Marsh, Phospholipid Bilayers: Physical Principles and Models, Wiley, New York, 1987.
[20] Z. An, G. Lu, H. Möhwald, J. Li, Self-assembly of human serum albumin (HSA) and L-α-dimyristoylphosphatidic acid (DMPA) microcapsules for controlled drug release, Chem. Eur. J. 10 (2004) 5848–5852.
[21] Z. An, C. Tao, G. Lu, H. Möhwald, S. Zheng, Y. Cui, J. Li, Fabrication and characterization of human serum albumin and L-α-dimyristoylphosphatidic acid microcapsules based on template technique, Chem. Mater. 17 (2005) 2514–2519.
[22] J. Li, Y. Zhang, L. Yan, Multilayer formation on a curved drop, Angew. Chem. Int. Ed. 40 (2001) 891–894.
[23] Z. Zhang, J.F. Rusling, Electron transfer between myoglobin and electrodes in thin films of phosphatidylcholines and dehexadecylphosphate, Biophys. Chem. 63 (1997) 133–146.
[24] Y. Wu, S. Hu, Direct electron transfer of ferritin in dihexadecylphosphate on an Au film electrode and its catalytic oxidation toward ascorbic acid, Anal. Chim. Acta 527 (2004) 37–43.
[25] H. Liu, L. Wang, N. Hu, Direct electrochemistry of hemoglobin in biomembrane-like DHP–PDDA polyion–surfactant composite films, Electrochim. Acta 47 (2002) 2515–2523.
[26] L. Wang, N. Hu, Electrochemistry and electrocatalysis with myoglobin in biomembrane-like DHP–PDDA polyelectrolyte–surfactant complex films, J. Colloid Interface Sci. 236 (2001) 166–172.
[27] A. Bellelli, G. Antonini, M. Brunori, B.A. Springer, S.J. Sligar, Transient spectroscopy of the reaction of cyanide with ferrous myoglobin: effect of distal side residues, J. Biol. Chem. 265 (1990) 18898–18901.

[28] J.C. Kendrew, R.E. Dickerson, B.E. Strandberg, R.G. Hart, D.R. Davies, D.C. Phillips, V.C. Stone, Structure of myoglobin: a three dimensional Fourier synthesis at 2 Å resolution, Nature 185 (1960) 422–427.
[29] G. Sauerbrey, Use of quartz vibration for weighing thin films on a microbalance, Z. Phys. 155 (1959) 206–214.
[30] J. Brandrup, E.H. Immergut (Eds.), Polymer Handbook, Wiley, New York, 1975, part 5.
[31] T.E. Creighton (Ed.), Protein Structure: A Practical Approach, IRL Press, New York, 1990, p. 43.
[32] B.W. Gregory, D. Vaknin, J.D. Gray, B.M. Ocko, P. Stroeve, T.M. Cotton, W.S. Struve, Two-dimensional pigment monolayer assemblies for light harvesting applications: structural characterization at the air/water interface with X-ray specular reflectivity and on solid substrates by optical absorption spectroscopy, J. Phys. Chem., B 101 (1997) 2006–2019.
[33] H.A.O. Hill, Bio-electrochemistry, Pure Appl. Chem. 59 (1987) 743–748.
[34] R.W. Murray, in: A.J. Bard (Ed.), Electroanalytical Chemistry, vol. 13, Marcel Dekker, New York, 1984, pp. 191–368.
[35] M. Majda, in: R.W. Murray (Ed.), Molecular Design of Electrode Surfaces, Wiley, New York, 1992, pp. 159–206.
[36] A.J. Bard, L.R. Faulkner, Electrochemical Methods, 2nd Ed.Wiley, New York, 2001.
[37] J.J. O'Dea, J.G. Osteryoung, Characterization of quasi-reversible surface processes by square-wave voltammetry, Anal. Chem. 65 (1993) 3090–3097.
[38] A.-E.F. Nassar, Z. Zhang, N. Hu, J.F. Rusling, T.F. Kumosinski, Proton-coupled electron transfer from electrodes to myoglobin in ordered biomembrane-like films, J. Phys. Chem., B 101 (1997) 2224–2231.
[39] A.M. Bond, Modern Polarographic Methods in Analytical Chemistry, Dekker, New York, 1980.
[40] H. Ma, N. Hu, J.F. Rusling, Electroactive myoglobin films grown layer-by-layer with poly(styrenesulfonate) on pyrolytic graphite electrodes, Langmuir 16 (2000) 4969–4975.
[41] A.-S. Yang, B. Honig, Structural origins of pH and ionic strength effects on protein stability: acid denaturation of sperm whale apomyoglobin, J. Mol. Biol. 237 (1994) 602–614.
[42] C.P. Andrieux, C. Blocman, J.M. Dumas-Bouchiat, J.M. Saveant, Heterogeneous and homogeneous electron transfers to aromatic halides: an electrochemical redox catalysis study in the halobenzene and halopyridine series, J. Am. Chem. Soc. 101 (1979) 3431–3441.
[43] C.P. Andrieux, C. Blocman, J.M. Dumas-Bouchiant, F. M'Halla, J.M. Saveant, Homogeneous redox catalysis of electrochemical reactions: part V. Cyclic voltammetry, J. Electroanal. Chem. 113 (1980) 19–40.
[44] Z. Zhang, S. Chouchane, R.S. Magliozzo, J.F. Rusling, Direct voltammetry and catalysis with mycobacterium tuberculosis catalaseperoxidase, peroxidases, and catalase in lipid films, Anal. Chem. 74 (2002) 163–170.
[45] R. Huang, N. Hu, Direct electrochemistry and electrocatalysis with horseradish peroxidase in Eastman AQ films, Bioelectrochemistry 54 (2001) 75–81.
[46] H. Theorell, A. Ehrenberg, Spectrophotometric, magnetic, and titrimetric studies on the heme-linked groups in myoglobin, Acta Chem. Scand. 5 (1951) 823–848.
[47] P. Gerorge, G. Hanania, The ionization of acidic metmyoglobin, Biochem. J. 52 (1952) 517–523.
[48] H. Torii, M. Tasumi, in: H.H. Mantsch, D. Chapman (Eds.), Infrared Spectroscopy of Biomolecules, John Wiley & Sons, New York, 1996, pp. 1–18.
[49] J.F. Rusling, T.F. Kumosinski, Nonlinear Computer Modeling of Chemical and Biochemical Data, Academic Press, New York, 1996, pp. 117–134.